CHANDRA
X-ray Center 60 Garden St., Cambridge Massachusetts 02138 USA

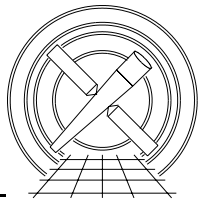

MEMORANDUM

Date: August 11, 2004
From: Richard J. Edgar and Alexey A. Vikhlinin
To: ACIS Team
Subject: Absolute QE of ACIS S1, S2 and S3 from XRCF data at selected energies
Cc: CXC Calibration Group
File: `memo.tex`
Version: `1.1`

---

1 Abstract

For some time now, it has been apparent that the ratio of the quantum efficiency (QE) of the Back Illuminated (BI) and Front-Illuminated (FI) chips in the ACIS camera was incorrect. We resolve this discrepancy by the analysis of ground calibration data, and discuss new curves for the BI quantum efficiencies.

The absolute quantum efficiency (QE) of ACIS chips S2 and S3 is derived at several energies from flat field data taken at the X-Ray Calibration Facility (XRCF). The data were taken in May 1997. Absolute quantum efficienty is derived by comparing count rates of the ACIS chips (derived from high-speed tap data) and a Flow Proportional Counter (FPC) in the target line. The FPC in question (fpc_hn) was absolutely calibrated at the synchrotron at BESSY.

We find that the Back-Illuminated chips S1 and S3 had their QE underestimated in released (version N0003) CALDB products, and discuss a corrected product. These curves have been released in Summer 2004 as version number N0005 of the ACIS QE files.

The sense and size of this correction is approximately what is needed for consistency with grating measurements (Marshall et al. 2003) and for some of the ACIS imaging mode observations of clusters of galaxies.

This memo has nothing to do with contamination of ACIS, but rather addresses the QE of ACIS at the time of launch.

2 Introduction

For some time now, it has been apparent that the ratio of the quantum efficiency (QE) of the Back Illuminated (BI) and Front-Illuminated (FI) chips in the ACIS camera was incorrect. One such line of evidence is detailed by Marshall et al. (2003). We resolve this discrepancy by the analysis of ground calibration data, and discuss new curves for the BI quantum efficiencies.

The Absolute Quantum Efficiency numbers detailed here support the notion that the discrepancy has three causes. One is that, in the on-orbit radiation environment, cosmic rays tend to form large blooms on FI chips, creating an effective "dead area" of order 3.5% under most circumstances, which results in an effective decrement to the QE of these chips. This effect will be accounted for separately, by introducing it into the tool which creates Ancillary Response Functions (ARF) for ACIS.

Another effect is that, in creating a model for use in interpolating in energy, the channel stops were mistakenly left on the illuminated side of the BI chips. When this is corrected, the resulting curves fit

the low energy XRCF data much better. This results in a significant increase in the BI QE at energies below a few hundred eV.

The final effect has to do with the non-uniform QE over the BI chips at the time of launch. This is a Charge Transfer Inefficiency (CTI) effect. Since the fall of 1999 the FI chips also have significant CTI, but at launch it was immeasurably small, and the chips were accordingly quite uniform. Ground calibration data such as those analyzed here were used to compute the chip-averaged QE at a number of energies. A re-definition of the QE Uniformity factor (QEU) to make it unity near the readout necessitates a re-computation of the BI QE model at high energies where the QEU factor differs most strongly from unity. We have accordingly selected new QE curves with different depletion depths from those released before (N0003 in the CALDB), in order to account for the energy dependence of the chip-averaged QEU factor.

3 Experimental Setup

During Phase I (as in eye, not Roman Numeral One) at XRCF, starting in early May 1997, the HRMA had been removed. The ACIS flight camera was placed at or near the former HRMA focal point, and flat-field tests were run at a variety of energies used earlier during the HRMA/ACIS calibration.

The HXDS (HRMA X-ray Detection System; i.e. ground calibration instruments) equipment in place included four Flow Proportional Counters (FPC) Beam Normalization Detectors (BND) near the front of the HRMA in the main chamber (the BND-H), and two detectors (one FPC and one high-purity Germanium Solid State Detector [SSD]) in Building 500, much closer to the source building up the beam pipe.

Two of the BND detectors (the fpc_hn, [the north BND-H], and the fpc_5, the FPC in building 500) were on translation stages, and could be moved around in the beam to test its uniformity. The former fpc_x2, the FPC used at the focal point of the HRMA during the HRMA-only testing (Phases C, D, and E) in Dec 1996 through February 1997, was placed in the fpc_hs (south BND-H) position.

Four of the HXDS detectors were calibrated were calibrated absolutely at BESSY in the summer and fall of 1997. These include the ssd_5, the ssd_x (focal point detector not used in the Phase I flat field tests), the fpc_hn and the fpc_x2 (during Phase I mounted in the fpc_hs position).

Since for the present analysis we are interested in the absolute calibration of the ACIS flight chips, we will use the calibrated HXDS detectors to determine the intensity and uniformity of the x-ray beam, and compare the count flux of ACIS to the photon flux predicted by the simultaneous BND measurements. These should differ by a factor of the ACIS QE.

The source used for this experiment was the Electron Impact Point Source (EIPS), using various anodes, including iron, niobium, carbon, and a SiO_2 anode mounted on a copper base. The source high voltage was set such that the K or L line in question was excited (but low enough in the case of the SiO_2 anode to avoid exciting the Si K–α line. The resulting spectrum of this anode has been shown by LETG measurements to contain the Oxygen K–α line at 0.525 keV, the Cu L–α complex near 0.9297 keV, a Bremmsstrahlung continuum, and a weak carbon K line which ACIS cannot see. Line energies are taken from Bearden (Rev Mod Phys, 39, 78, 1967).

The other experiments included filters between the source and the detectors (physically located near the source in Building 600), which serve to absorb a large fraction of the continuum, making separation of the line fluxes easier even in low resolution detectors such as proportional counters. The carbon experiment used a plastic filter; the Nb experiment used a Zr filter, and the Fe experiment, targeting the Fe K–α line, used a Mn filter, which absorbs the Fe K–β line as well as the continuum.

Details of the HXDS calibration and beam uniformity test analysis can be found in the SAO report "XRCF Phase 1 Testing: Analysis Results," dated August 1999, and available on the web:

X_Ray_line	energy	S2	S3	BU
C−Kα	0.277	−−	I−IAS−EA−2.050	J−BND−BU−2.038
O−Kα	0.525	I−IAS−EA−2.004	I−IAS−EA−2.003	I−BND−BU−2.129
Cu−Lα	0.9297	I−IAS−EA−2.004	I−IAS−EA−2.003	I−BND−BU−2.129
Nb−Lα	2.166	I−IAS−EA−2.021	I−IAS−EA−2.022	J−BND−BU−2.014
Fe−Kα	6.4	I−IAS−EA−2.039	I−IAS−EA−2.040	J−BND−BU−2.028

Table 1: XRCF Tests analyzed for the absolute QE of the S2 and S3 chips, including the Beam Uniformity (BU) tests used. In addition one S1 test was analyzed, namely I-IAS-EA-2.038 at Fe–Kα.

`http://hea-www.harvard.edu/MST/simul/xrcf/report/index.html`

Of special interest are chapters 3 (HXDS Flow Proportional Counters) and 24 (EIPS Beam Uniformity).

The BND detectors were run continuously, and ACIS was run with the High Speed Tap (HST) attached to first one chip and then another. We will look at the S2 and S3 HST data for this initial analysis. The TRW_ID (test identifier) was changed whenever the HST was moved to another chip. The HXDS runid also changed at these times.

The tests analyzed and some of the experimental parameters are given in Table 1.

4 Analysis Procedure

4.1 Preparation of the ACIS data

The ACIS data were taken by the High Speed Tap, attached to one chip at a time. The full-frame data resulting from this were stored to disk (in the interests of space, they are archived on DLT tapes). Kenny Glotfelty then ran event finding software on them, producing FITS format event lists. These are still on the CfA disks, here: /data/acis1/xrcf/PHASE_I/ filed under date of observation and TRW_ID.

These event lists are not quite in modern Level 0 format, so they were processed by grading and pulse height summing software (Dan Nguyen's `addfltgradeadu2subass` program) which was written to handle data in this format. In addition, the header keyword `ONTIME` must be copied to `LIVETIME`.

The ciao tool `dmextract` can then be used to extract spectra, either for a whole chip (which was done for S2), or selected areas (the S1 and S3 data were extracted one node at a time). These are made into xspec-compatible PHA files, which are histograms of number of events vs. pulse height in ADU. 4096 channels were used in these extractions.

The HXDS instruments produce as raw data products histogrammed pulse height spectra in ASCII files, one per iteration. These are summed by a perl script, since many iterations were performed during the time that ACIS was exposed in each case. The resulting summed spectra were then converted to minimal FITS files for fitting in xspec.

The full details of the analysis are given by Edgar in a memo entitled "Absolute QE of ACIS S2 and S3 from XRCF data at Oxygen K–α and Copper L–α, dated Nov 13, 2003, for the oxygen and copper data; other analyses proceded in an analagous fashion. Notable systematics include the presence of a few percent of lead in the Mn filter (used in the Fe–Kα tests).

5 Results

We proceed to give the results. Let the countrate for a detector be C_{det} in units of cts s^{-1}. Each detector has an area, A_{det} in cm^2, a source distance d_{det} in cm. In addition, each detector has an

chip	energy	QE	QE_err
S3	0.277	0.3394	0.0110
S2	0.525	0.2279	0.0045
S3	0.525	0.6147	0.0117
S2	0.930	0.5577	0.0141
S3	0.930	0.8412	0.0242
S2	2.166	0.5939	0.0184
S3	2.166	0.8056	0.0253
S1	6.404	0.5027	0.0177
S2	6.404	0.8787	0.0311
S3	6.404	0.6855	0.0266

Table 2: Absolute, chip-averaged QE and statistical errors, derived from the XRCF flat-field data.

energy-dependent quantum efficiency, QE_{det}, which I find it useful to think of in units of cts photon^{-1}. For the BND detectors, these are taken from the BESSY calibration, as reported in Table 3.10 of the MST report *XRCF Phase 1 Testing: Analysis Results*. The QE of the ACIS chips is, of course, the goal of the present analysis. Furthermore, there is a beam uniformity correction for each detector position, BU_{det}.

For each detector then, the source luminosity is given by:

$$S = \frac{C_{det}}{A_{det} QE_{det}} \times d_{det}^2 BU_{det}$$

Since all detectors are looking at the same source at the same time, S is independent of the detector. Setting the two measurements of S equal, and solving for QE_{ACIS}, we obtain:

$$QE_{ACIS} = QE_{hn} \times \frac{C_{ACIS}}{C_{hn}} \times \frac{A_{hn}}{A_{ACIS}} \times \frac{BU_{ACIS}}{BU_{hn}} \times \frac{d_{ACIS}^2}{d_{hn}^2}$$

The ACIS area is taken from the POG, version 5.0, Table 6.1, which gives the pixel size as 24.0 microns. This is for the flight temperature, -120°C, while the XRCF measurements were done at -110°C. I neglect the thermal expansion. Each node is 256 × 1024 pixels, minus the edge rows and columns. This gives a total of 259,488 pixels, for a total area of 1.4952 cm^2 per node, or 5.9809 cm^2 for a whole chip.

We give final results in Table 2.

Note that the derived QE numbers at the Nb L–α line are systematically low for both the S2 and S3 chips. Some unknown systematic effect seems to be responsible for this underestimation.

One possible systematic effect we have neglected here concerns the finite width of fluorescent lines in electron impact sources, especially for low–Z elements such as oxygen. However, the LETG calibration included a measurement of the width of this line under slightly different circumstances (filter, high voltage) from this same source. They find that the flux in the line is down by more than two orders of magnitude before we get to the energy where the resonant absorption in the filter (and oxide layer on the CCD) occur near 0.53 keV. We therefore believe we are justified in neglecting this effect.

6 QE Models

The ACIS quantum efficiencies measured at the XRCF are *chip-averaged* quantities. If the charge transfer inefficiency (CTI) is strong, the grade distribution of the detected photons is altered. This

energy	Average QEU	
	S3	S1
0.277	0.998	0.993
0.525	0.994	0.968
0.930	0.989	0.942
2.166	0.964	0.852
6.404	0.928	0.806

Table 3: Average QEU correction for the calibration energies

results in misclassification of a certain fraction of the X-ray photons as the charged-particle events and their subsequent removal from the event lists. The effect is known as the grade migration.

The grade migration is stronger for the photons detected far from the CCD readout and therefore transfered for a greater distance. In ACIS CCDs, grade migration is virtually non-existent in the first ~ 100 rows adjacent to the readout, while it can be quite strong at the top 100 rows. Therefore, the grade migration leads to spatially-dependent detection efficiency. The CXC approach is to factorize the detection efficiency into the product of two components: (a) spatially-independent quantum efficiency (QE) of a perfect CCD (that without the CTI), and (b) the quantum efficiency non-uniformity corrections, also known as the QEU tables.

XRCF measurements provide the product of the QE and the average QEU for the given CCD. The calibration products require the QE part, so a further correction must be made. At the time of the XRCF calibration, this problem affected only the BI chips because the FI CCDs had essentially zero CTI and therefore, QEU = 1.

To obtain the QE for "ideal" CCDs, we need to divide the chip-averaged values from Table 2 by the average QEU correction at the given energy,

$$\mathrm{QE}_0 = \frac{\mathrm{QE}}{\langle \mathrm{QEU} \rangle}$$

We have developed an accurate model for the QEU, both as a function of location and energy. The average corrections given by this model are listed in Table 3.

The QEU correction is rather strong at high energies ($\sim 10-20\%$ for the Fe-K line at 6.404 keV) and it moves the measured QE values above the prediction of the previously adapted CCD model. Therefore, the model must be updated. The model parameter that affects the high-energy QE most strongly is the thickness of the depletion layer. The previously adapted thicknesses are 30μm for S1 and 41μm for S3 (these values were obtained by fitting the preliminary QE measurements). We find that to satisfy the absolute QE measurements at the XRCF, the depletion thicknesses must be slightly increased, to 36μm in S1 and 46μm in S3. We incorporate these values in the updated QE model distributed to the *Chandra* users.

With these corrections, it is possible to compare the chip-averaged QE numbers measured above, with the intrinsic chip QE which is found in the CALDB QE files. We first divide the chip average QE numbers from Table 2 by the mean QEU from Table 3. These numbers are then plotted on the same axes as the QE curves from the CALDB, as they represent the intrinsic chip QE, prior to any degradation or event loss due to CTI effects. We show these plots in figures 1 and 2. Note the excellent agreement with the new QE curves, which will be released in summer 2004 as version N0005, and the improvement relative to the existing product, N0003. The exception to this, noted above, is the Nb L–α measurement at about 2.1 keV, which systematically underestimates the QE for reasons that are not clear at present.

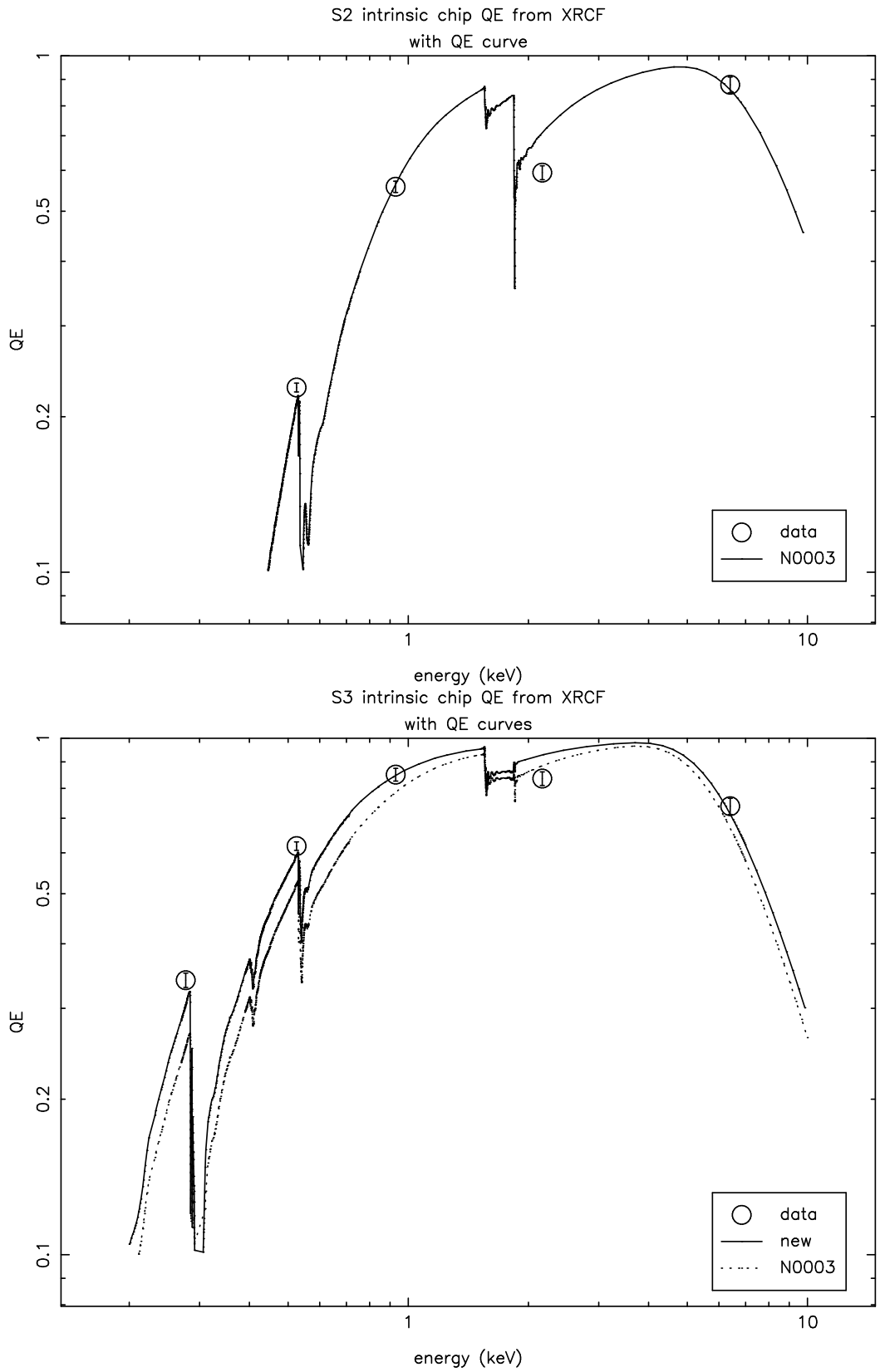

Figure 1: S2 and S3 corrected QE, compared with the existing CALDB curve (N0003, dotted) and the new CALDB curve, N0005.

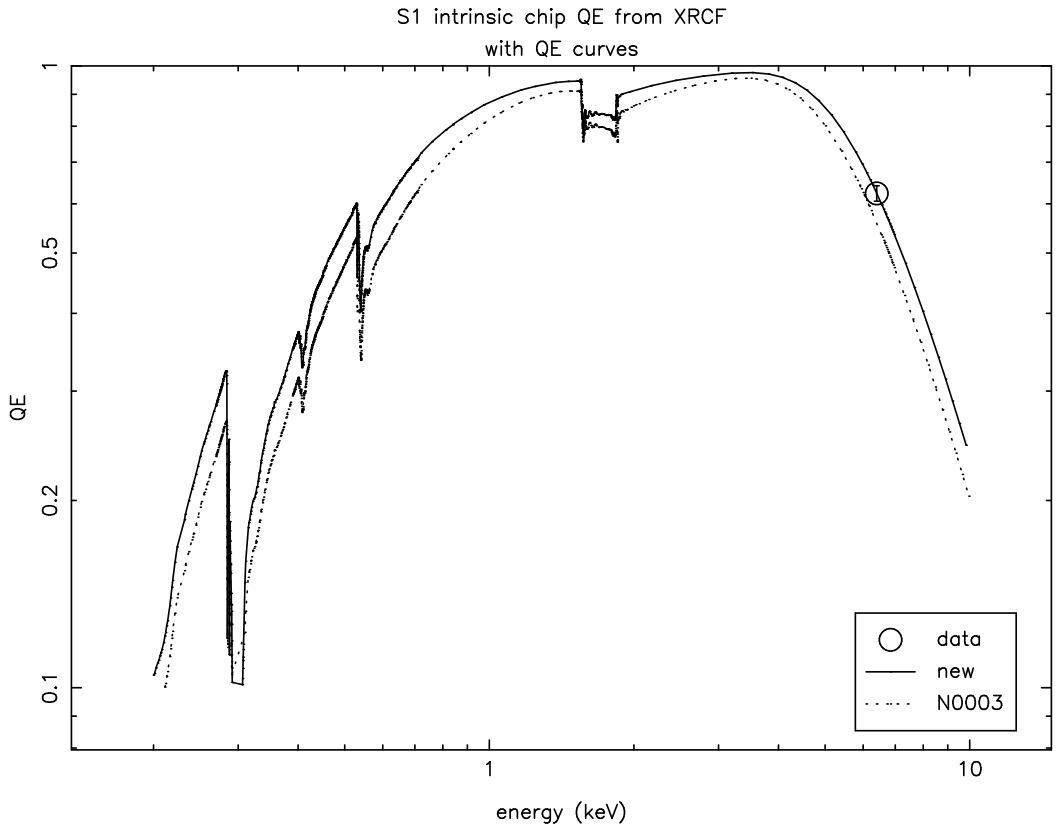

Figure 2: S1 corrected QE, compared with the existing CALDB curve (N0003, dotted) and the new CALDB curve, N0005.

7 References

- Butt, Yousaf and Spitzbart, Brad, "ACIS Cosmic Ray Induced Dead Area," Internal CXC Memo.
- Edgar, Richard, "Absolute QE of ACIS S2 and S3 from XRCF data at Oxygen K–α and Copper L–α, dated Nov 13, 2003, http://cxc.harvard.edu/cal/Acis/Cal_prods/qe/ACIS_QE_O_S23.ps
- Marshall, Herman, Dewey, Daniel., and Ishibashi, Kazunori "In-Flight Calibration of the Chandra High Energy Transmission Grating Spectrometer," SPIE, 5165, 457 (2003). Also available at: http://xxx.lanl.gov/abs/astro-ph/0309114